Nanoscale

Dynamic Article Links ►

www.rsc.org/nanoscale

ESI for DOI:10.1039/c1nr10884k

Scalable processes for fabricating non-volatile memory devices using self-assembled 2D arrays of gold nanoparticles as charge storage nodes

Electronic Supplementary Information

Girish Muralidharan,[a] Navakanta Bhat*[b] and Venugopal Santhanam*[a]

Received 20th July 2011, Accepted 13th September 2011

DOI: 10.1039/c1nr10884k

Experimental Details

Gold nanoparticle synthesis. Aqueous gold colloids of size 7 ± 0.7 nm were synthesized at room temperature using tannic acid as both reducing and stabilizing agent, as reported earlier[S1]. Briefly, 30 mL of 0.64 mM aqueous chloroauric acid was added to 45 mL of 0.9 mM aqueous tannic acid drop wise. The pH of the reaction mixture was always maintained above 6.4 by the addition of requisite amounts of 1 % (w/v) KOH solution intermittently. Particles of different size (5 ± 0.7 nm) were obtained by scaling the amount of chloroauric acid added. Dodecanethiol capping of gold nanoparticles was accomplished by mixing 5 mL ethanol solution (containing 5 µL dodecanethiol) with 5 mL of aqueous gold colloid, maintained at a pH of 4. The solution was left undisturbed for 2 hours, and then centrifuged at 3500 rpm for 30 minutes. The precipitate was then washed with 5 mL ethanol twice to remove uncapped dodecanethiol molecules. The final precipitate was dispersed in 0.4 mL of toluene (5 nm particles) or 1:3 (volume) chloroform-toluene mixture (7 nm particles), prior to array formation. However, larger size particles could be suspended in pure toluene by increasing the ligand length (results not shown). The ability to disperse larger particles arises either due to the enhanced screening of interparticle van der Waals attraction by using a higher dielectric constant medium (i.e. adding chloroform) or by reducing the magnitude of attractive interactions due to an increase in the interparticle separation at contact (i.e. longer ligands)[S2].

Device fabrication. Silicon wafer (p-type, (100) orientation, resistivity of 1-2 Ω.cm) was cleaned using standard RCA (Radio Corporation of America) method[S3] followed by HF (Hydrofluoric acid) dip to remove the native oxide. A 10 nm oxide layer was thermally grown on the wafer by dry oxidation at 950 °C for 5 minutes. Subsequently, sample was annealed at 950 °C for 20 minutes under nitrogen environment, to passivate the interface traps. Ellipsometry (Sentech) measurements confirmed the oxide thickness. Ohmic back contacts were formed by thermal evaporation (HindHivac 15F6) of 100 nm thick aluminium (after carefully removing the oxide using buffered HF solution), and subsequent post-deposition annealing at 450 °C for 20 minutes under forming gas environment. After microcontact printing of gold nanoparticle array, gadolinium oxide was sputter-deposited using RF magnetron sputtering unit (Anelva SPF-332H) followed by thermal annealing at 500°C for 30 min under forming gas environment. All these fabrication processes were carried out in a class 1,000 cleanroom. For device characterization, 300 µm diameter aluminium contacts with ~100 nm thickness were deposited on the top surface (gate electrode) by thermal evaporation through a shadow mask, followed by post-deposition annealing at 450 °C for 30 minutes for improving the contact between aluminium and oxide.

Sample Characterization. Room temperature, high frequency (1 MHz), capacitance-voltage (CV) and capacitance time (Ct) measurements were carried out using Agilent HP 4284A CV meter. The delay and hold time at each measurement point were set to 100 ms during CV characterization. P/E voltages of ∓ 7 V were used for retention and endurance characterization. For retention characterization, P/E voltages were applied for 10 s duration initially, and then the capacitance values were measured ('reading') at −0.8 V (initial flatband voltage). The pulse widths of P/E voltages during endurance characterization were set at 100 ms; use of longer durations resulted in the same value for threshold voltage shifts. Field-Emission Scanning Electron Microscope (FESEM) images were obtained using Ultra-55, Zeiss NTS GmbH, at an operating voltage of 10 to 15 kV. Multiple images taken at different locations were used for image analysis and size determination. The images presented were taken in SE (Secondary Electron) mode, unless stated otherwise. EFM characterization was performed using an Asylum Research-MFP 3D instrument at 21°C and 45% RH. A set of platinum coated silicon tips (Olympus, OMCL-AC-240 TM, spring constant: 2 N/m, resonant frequency: 70 kHz) were used for imaging and EFM measurements. First, AFM topography scan was performed on the substrate using tapping mode. Then, charge was injected at -6 V for 2 min by placing the tip in contact with the nanoparticle array embedded in gadolinium oxide (programming). Immediately afterwards, the AFM tip was taken to a height of 80

---

[a] *Department of Chemical Engineering, Indian Institute of Science, Bangalore, 560012, India. Fax: +91-80-2360 8121; Tel: +91-80-2293 3113;*E-mail: venu@chemeng.iisc.ernet.in*

[b] *Department of Electrical Communication Engineering and Centre for Nanoscience and Engineering, Indian Institute of Science, Bangalore, 560012, India. Fax: +91-80-2360 6475; Tel: +91-80-2293 2279;*E-mail: navakant@ece.iisc.ernet.in*

nm above the surface and scanned by retracing the AFM topography recorded earlier, while applying a tip voltage of 3 V (reading). Localized negative/positive charges result in attractive/repulsive forces, which can be seen as changes in phase lag i.e. the phase lag between applied signal and tip oscillation. Scanning 80 nm above the surface helps in eliminating van der Waals interactions and capturing only long-range electrostatic effects. X-ray photoelectron spectroscopic (XPS) spectra were measured using a Thermo Scientific Multilab-2000 instrument with Al Kα (energy of 1486.6 eV) as the X-ray radiation source. XPS spectra were fitted using Fityk software (http://fityk.nieto.pl)[S4].

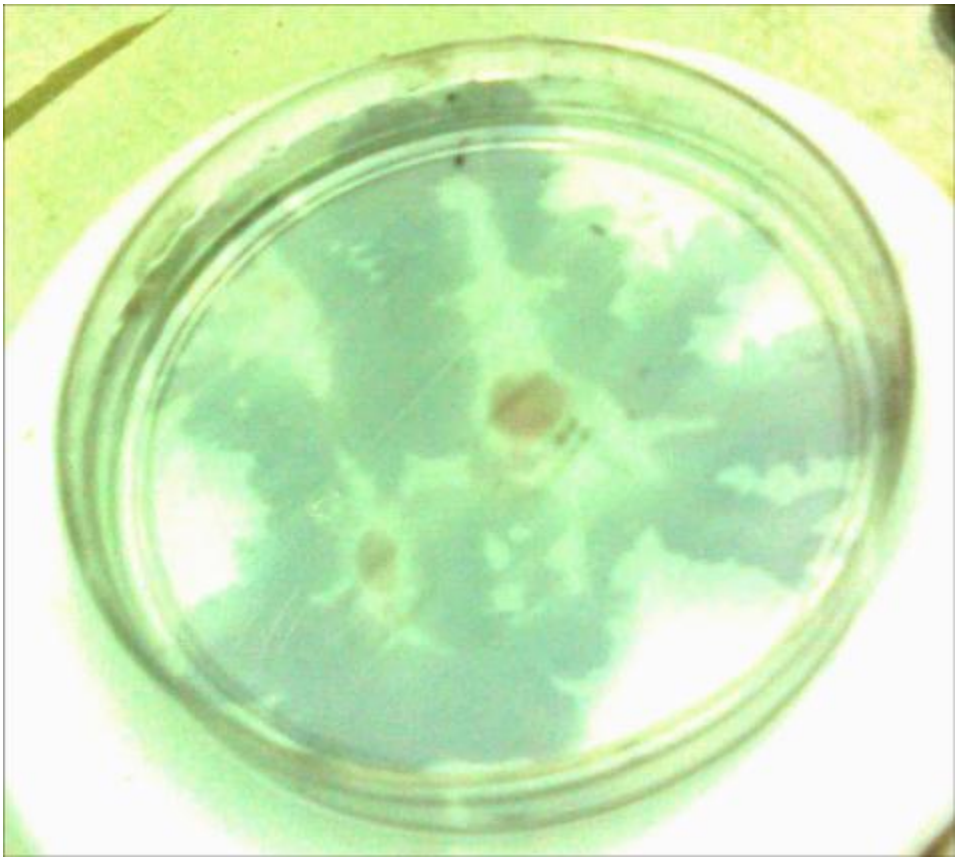

Fig. S1 Digital photograph of an array formed by spreading a drop of a colloidal solution of dodecanethiol coated gold nanoparticles in toluene, without excess dodecanethiol, on a water surface. The drop does not spread into a uniform thin film and also dewets at the later stages into multiple daughter drops (visible near the center of the image). The arrays formed after drying are also not uniform and consist of monolayer and multilayer domains.

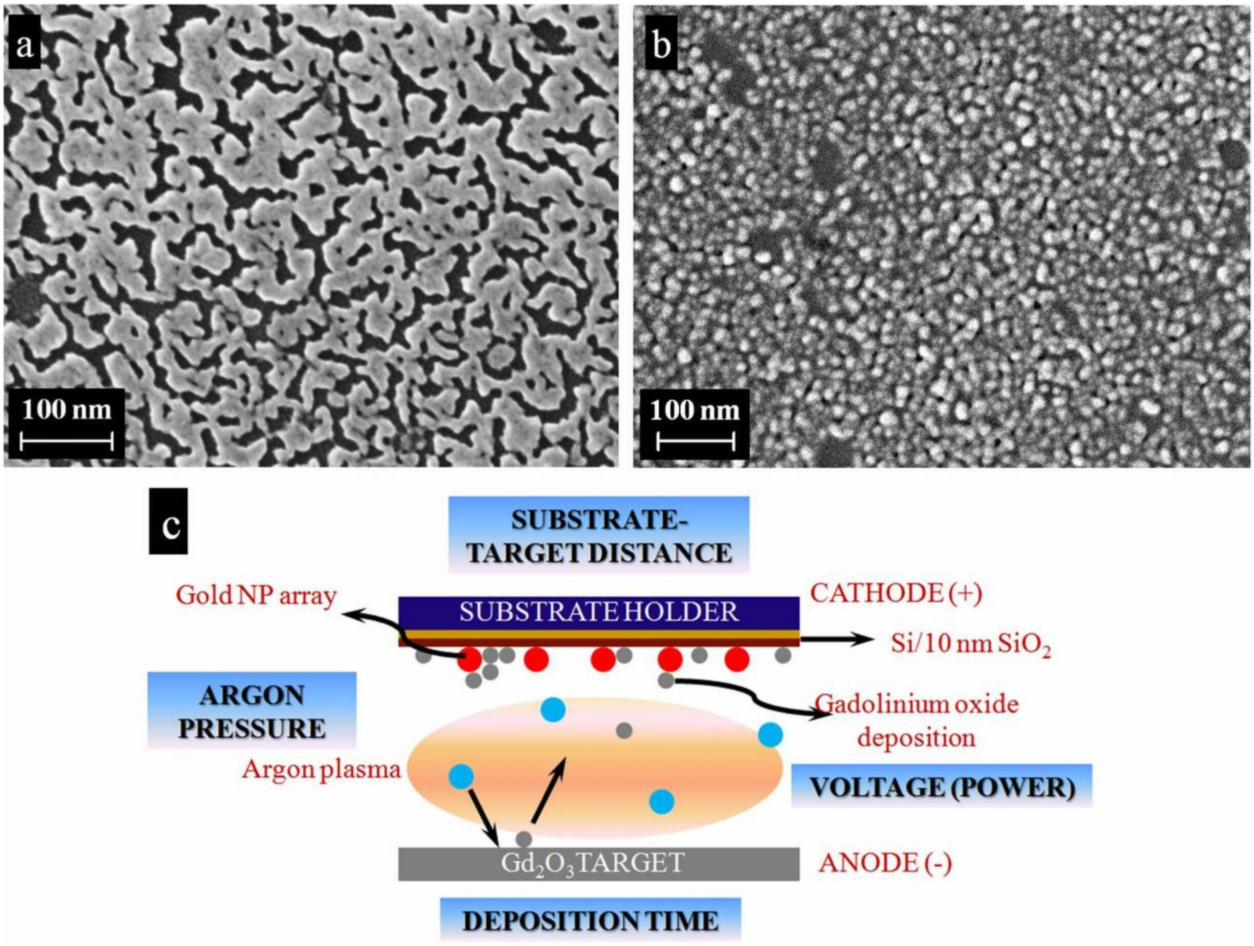

Fig. S2 Effect of RF sputtering conditions on dodecanethiol capped gold nanoparticle array during gadolinium oxide deposition. (a) Use of higher Argon pressure (~0.01 mbar) led to fusion of nanoparticles into percolating thin sheets while (b) higher voltage (~2 kV) resulted in coarsening of nanoparticles. (c) Schematic of the RF magnetron sputtering process for gadolinium oxide deposition, indicating the various parameters that were optimized in this study.

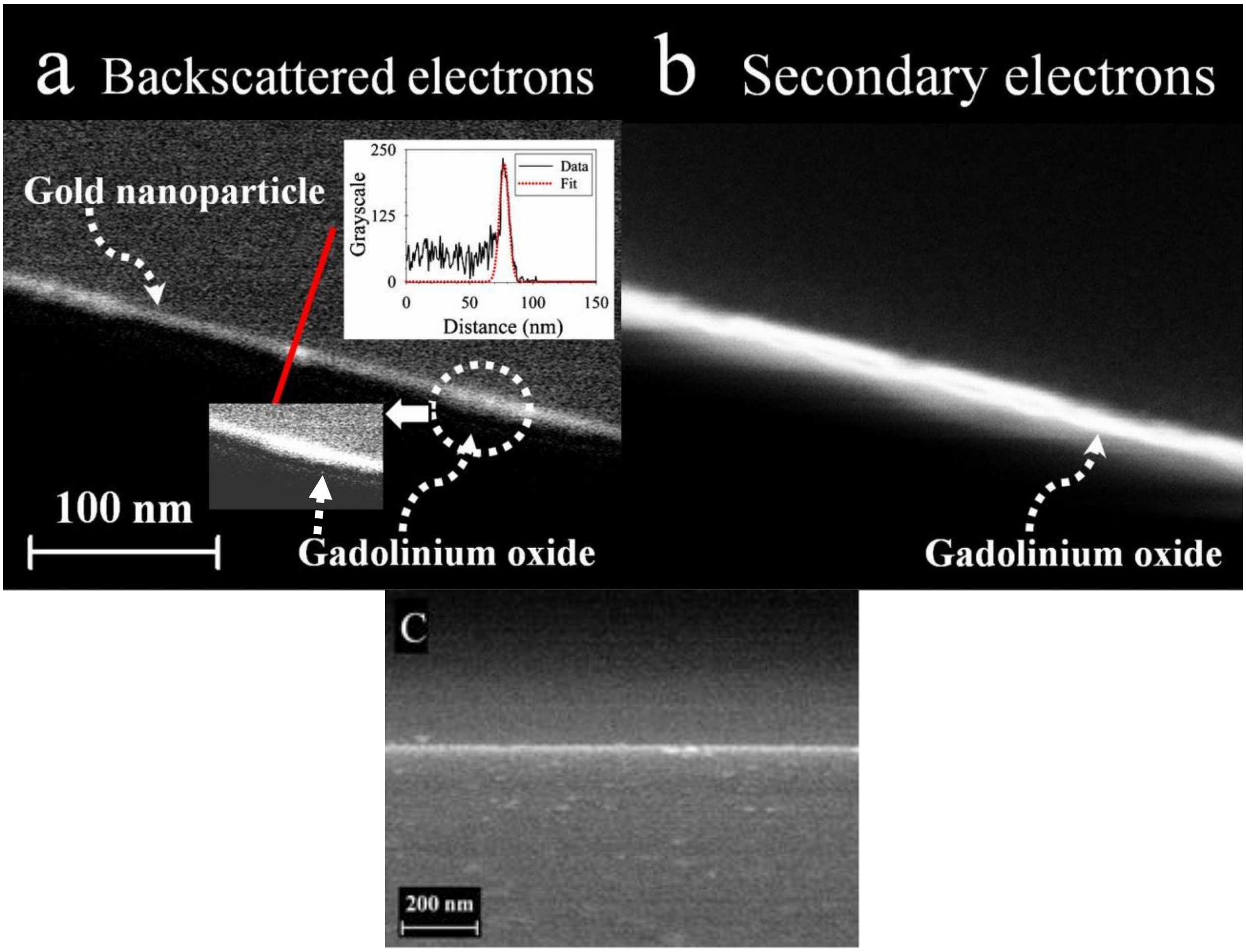

Fig. S3 C Representative high magnification cross-sectional FESEM images of the MOS capacitor with gold nanoparticle arrays as charge storage nodes, obtained using (a) angle selective backscattered electron (AsB) and (b) secondary electron (SE) detector. Contrast in backscattered electron imaging is predominantly due to the difference in atomic weight (Z) while secondary electron imaging depends on surface features. Here, the sample contains both gold (Z = 197) and gadolinium oxide (Z = 363.49/5=72), hence gold nanoparticles are seen clearly in AsB and not using SE detector. The edge of the sample appears as a very faint line (indicated by the arrow labelled gadolinium oxide) in (a), while it appears very bright in (b) due to the predominance of edge effects in SE imaging. A 2-D profile plot of the grayscale values across the MOS capacitor (inset in figure a) indicates the thickness of array to be ~ 7 nm, based on full width at half maximum. (c) Low magnification cross-sectional FESEM image of the MOS capacitor, obtained using angle selective backscattered electron detector indicating large scale uniformity. The dense packing of the array precludes visualization of individual nanoparticles. These samples were obtained by cleaving the silicon substrate.

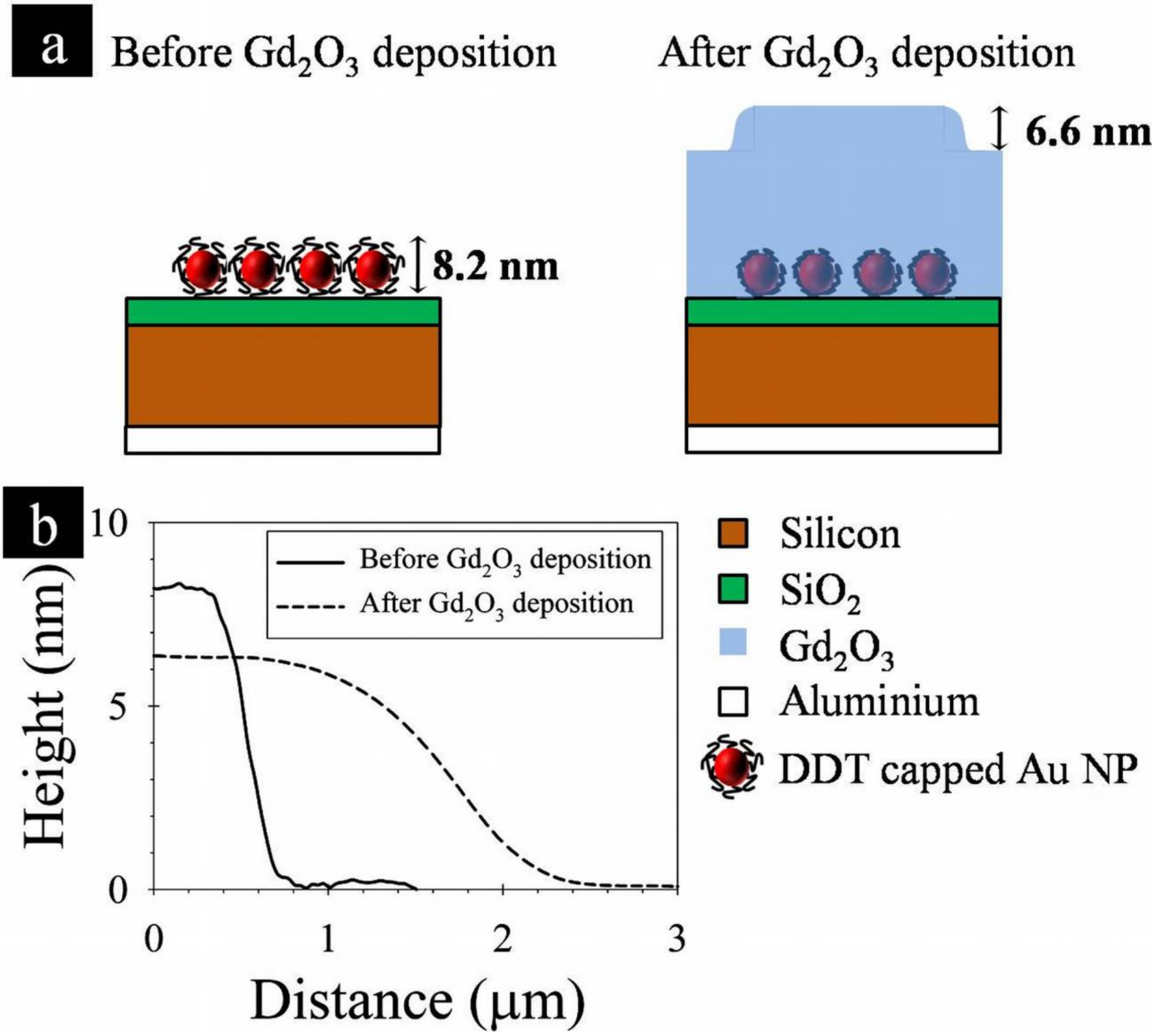

Fig. S4 (a) Schematic illustrating the expected cross-section of the device before and after RF sputter deposition, indicating that most of the ligand molecules have been removed from the ligand layer after gadolinium deposition. (b) AFM cross-sectional height profiles across the edge of the 5 nanoparticle array before and after gadolinium oxide deposition by RF sputtering. A decrease in the difference of height from 8.2 nm to 6.6 nm indicates that most of the ligands have been removed during the RF sputtering process.

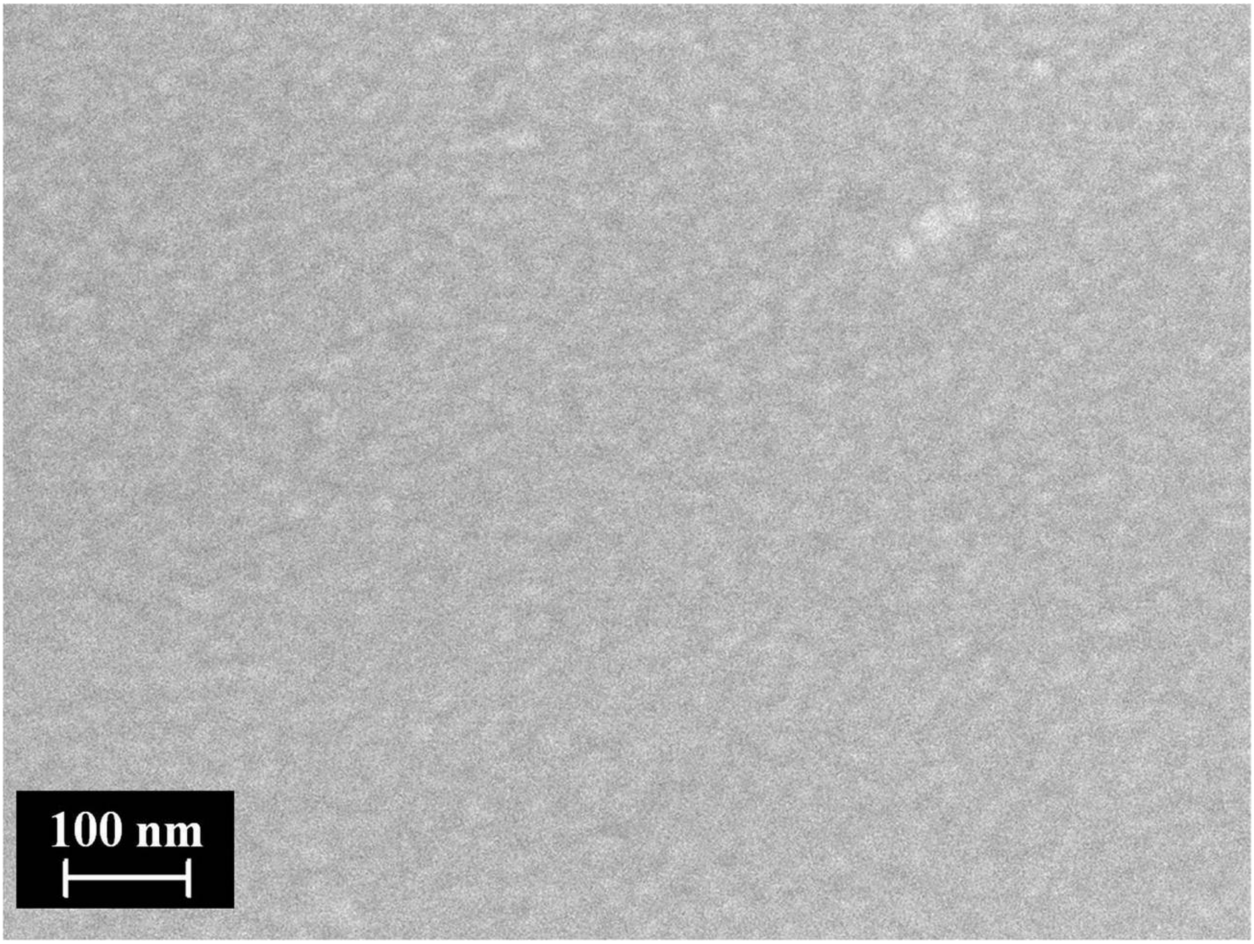

Fig. S5 Representative FESEM image of MOS capacitor fabricated with a 30 nm thick gadolinium oxide layer, indicating poor lateral resolution, which hinders the visualization of the in-plane ordering of the nanoparticle array.

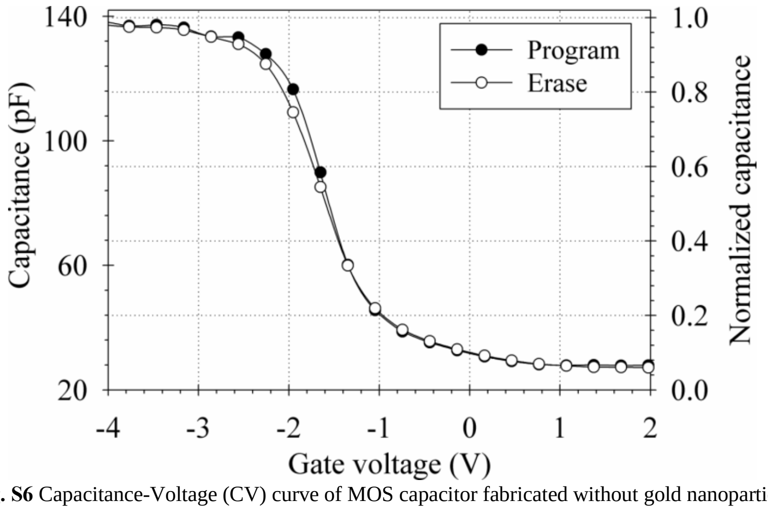

Fig. S6 Capacitance-Voltage (CV) curve of MOS capacitor fabricated without gold nanoparticles (control sample), indicating negligible hysteresis.

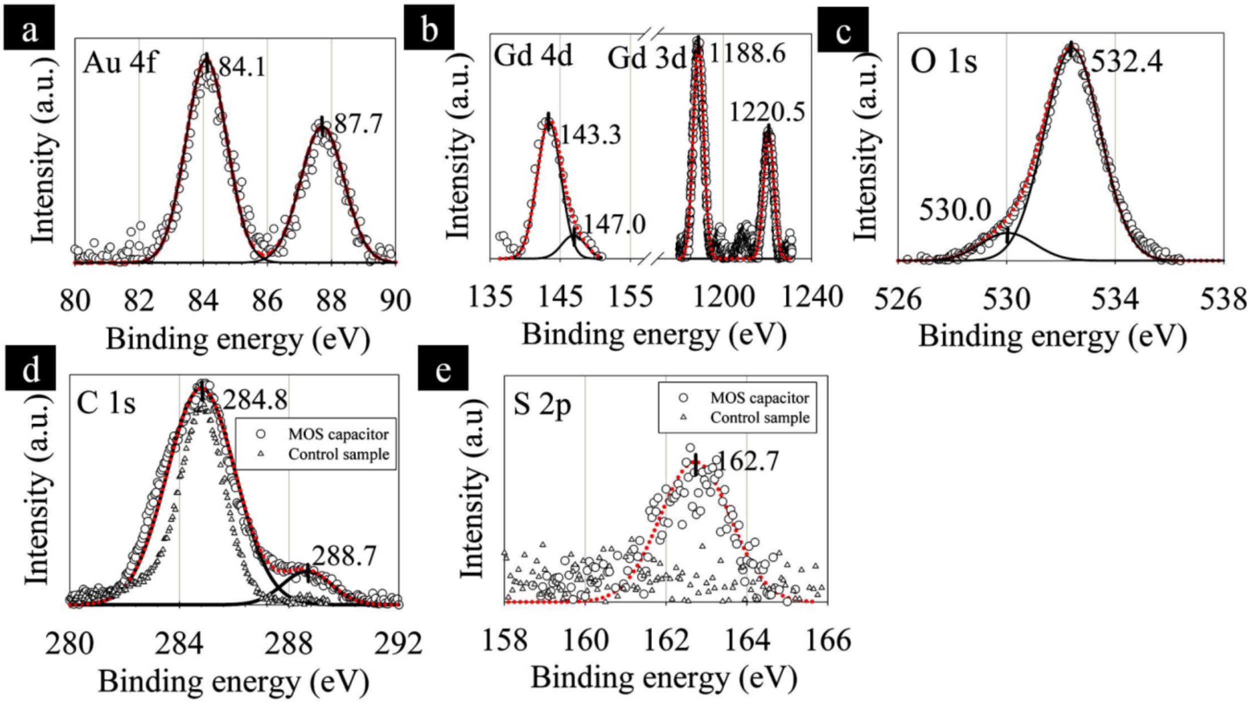

Fig. S7 (a) Au 4f Core level XPS spectrum from a MOS capacitor with embedded nanoparticle array indicating the presence of gold in metallic form (84.1 and 87.7 eV). XPS spectra of (b) Gadolinium 3d and 4d levels, and (c) Oxygen 1s level indicate the predominant presence of hydroxide (532.4 eV), possibly as gadolinium hydroxide ($Gd(OH)_3$) and is attributed to the hygroscopic nature of rare earth oxides. XPS spectra of (d) Carbon 1s and (e) Sulphur 2p core levels for MOS capacitors fabricated with and without (control) gold nanoparticle arrays embedded in gadolinium oxide. For MOS capacitors with the embedded nanoparticle array, the presence of C=O (288.7 eV) and trace amount of sulphur (162.7 eV) indicates that some residual ligands are trapped inside. C=O bonds are expected to have formed during the annealing steps by decomposition of the trapped ligands. In these figures, the symbols represent measured data points, the black lines represent deconvoluted peaks, and the red lines represent the overall fit. The numbers in the panels represent the peak values of the fitted curves.

References

S1 S. K. Sivaraman, S. Kumar and V. Santhanam, *Gold Bull.*, 2010, **43**, 275.

S2 B. A. Korgel, S. Fullam, S. Connolly and D. Fitzmaurice, *J Phys Chem B*, 1998, **102**, 8379.

S3 W. Kern and D. A. Puotinen, *RCA Review*, 1970, **31**, 187.

S4 M. Wojdyr, *J. Appl. Crystallogr.*, 2010, **43**, 1126.